Letter

Thermalization at the femtoscale seen in high-energy Pb+Pb collisions

Rupam Samanta,[1,2] Somadutta Bhatta,[3] Jiangyong Jia,[3,4] Matthew Luzum,[5] and Jean-Yves Ollitrault[2]

[1]*AGH University of Science and Technology, Faculty of Physics and Applied Computer Science, Aleja Mickiewicza 30, 30-059 Cracow, Poland*

[2]*Université Paris Saclay, CNRS, CEA, Institut de Physique Théorique, 91191 Gif-sur-Yvette, France*

[3]*Department of Chemistry, Stony Brook University, Stony Brook, New York 11794, USA*

[4]*Physics Department, Brookhaven National Laboratory, Upton, New York 11976, USA*

[5]*Instituto de Física, Universidade de São Paulo, Rua do Matão, 1371, Butantã, 05508-090, São Paulo, Brazil*

(Received 8 May 2023; revised 8 January 2024; accepted 16 April 2024; published 3 May 2024)

A collision between two atomic nuclei accelerated at a speed close to that of light creates a dense system of quarks and gluons. Interactions among them are so strong that they behave collectively like a droplet of fluid of ten-femtometer size, which expands into the vacuum and eventually fragments into thousands of particles. We report a new manifestation of thermalization in recent data from the Large Hadron Collider. Our analysis is based on results from the ATLAS Collaboration, which has measured the variance of the momentum per particle across Pb+Pb collision events with the same particle multiplicity. This variance decreases steeply over a narrow multiplicity range corresponding to central collisions. We provide a simple explanation of this newly observed phenomenon: For a given multiplicity, the momentum per particle increases with increasing impact parameter. Since a larger impact parameter goes along with a smaller collision volume, this in turn implies that the momentum per particle increases as a function of density, which is a generic consequence of thermalization. Our analysis provides the first direct evidence of this phenomenon at the femtoscale.

DOI: 10.1103/PhysRevC.109.L051902

Nucleus-nucleus collisions carried out at particle colliders display phenomena of macroscopic nature, which are unique in the realm of high-energy physics [1,2]. These emergent phenomena occur due to a large number of created particles and to the nature of the strong interaction. A head-on collision between two ^{208}Pb nuclei at the Large Hadron Collider (LHC), at 5.02 TeV per nucleon pair (the current energy for ion beams), produces some 35000 hadrons [3], a fraction of which are seen in detectors. The emission of hadrons is the final outcome of a number of successive stages [1], one of which is the production of a state of matter called the quark-gluon plasma. In this phase, quarks and gluons, which are the elementary components of hadrons, are liberated [4]. They carry color charges, unlike hadrons, which are colorless. Interactions induced by these charges are so strong that they behave collectively like a fluid [5].

Transient formation of a fluid in nucleus-nucleus collisions has been inferred from the observation that particles move collectively into preferred directions, suggesting that their motion is driven by pressure gradients inherent in a fluid. Most notably, one observes an elliptic deformation of the azimuthal distribution of outgoing particles [6,7], which originates from the almond shape of the overlap area between the colliding nuclei (Fig. 1). These observations are reproduced by calculations using relativistic hydrodynamics to model the expansion of the fluid [8], which has become the standard description of nucleus-nucleus collisions.

Here, we report independent confirmation of the formation of a fluid, which does not involve the directions of outgoing particles, but solely their momenta. The ATLAS Collaboration at the LHC detects charged particles in an inner detector, which covers roughly the angular range $10^\circ < \theta < 170^\circ$ (where θ is the angle between the collision axis and the direction of the particle) and measures their transverse momenta $p_t \equiv p \sin\theta$. The analysis includes all charged particles detected in the interval $0.5 < p_t < 5$ GeV/c. The observables of interest are, for every collision, the multiplicity of charged particles seen in the inner detector, denoted by $N_{\rm ch}$, and the transverse momentum per charged particle, $(\sum p_t)/N_{\rm ch}$, denoted by $[p_t]$. $N_{\rm ch}$ is used to estimate the centrality [9–12], since a more central collision, with a smaller impact parameter produces on average more particles.

For collisions with the same $N_{\rm ch}$, $[p_t]$ fluctuates from event to event. After subtracting trivial statistical fluctuations, the remaining dynamical fluctuations [13] are very small, below 1% in central Pb+Pb collisions at the LHC [14]. These small dynamical fluctuations are the focus of our study. The left panel of Fig. 2(c) displays their variance as a function of $N_{\rm ch}$ [27]. The striking phenomenon is a steep decrease, by a factor $\approx$2, over a narrow interval of $N_{\rm ch}$ around 3700. This behavior is not reproduced by models of the collision in which the Pb+Pb collision is treated as a superposition of independent nucleon-nucleon collisions, such as the HIJING model [28,29], where the decrease of the variance is proportional to $1/N_{\rm ch}$ [14,30] for all $N_{\rm ch}$.

We will argue that the impact parameter, b, plays a crucial role in this phenomenon. The relation between $N_{\rm ch}$ and b is not one to one, and $[p_t]$ depends on both quantities. In order to illustrate this dependence, we simulate 150 collisions at $b = 0$ using relativistic viscous hydrodynamics, and evaluate

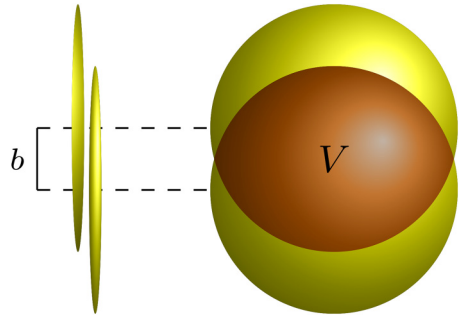

FIG. 1. Schematic representation of a collision between two identical spherical nuclei at impact parameter b. Left: Incoming nuclei just before the collision, flattened by the relativistic Lorentz contraction in the direction of motion. Right: View from the collision axis. Strongly interacting matter is created in the region where the nuclei overlap, which is indicated in darker color, and V is the collision volume. Generally, smaller b is associated with larger V.

$N_{\rm ch}$ and $[p_t]$ for every collision. Figure 3 displays their distribution. The first observation is that they span a finite range. Fluctuations around the mean extend up to ≈14% for $N_{\rm ch}$, and to ≈3% for $[p_t]$. They originate from quantum fluctuations at different levels: In the positions of nucleons at the time of impact [32], in the partonic content of the nucleons [33], and in the process of particle production.[1] Modern hydrodynamic simulations take these fluctuations into account [36] by implementing a different initial density profile (the initial condition of hydrodynamic equations) in every collision. The second observation in Fig. 3 is that there is a positive correlation between $[p_t]$ and $N_{\rm ch}$ in hydrodynamics.

This correlation is a consequence of local thermalization, which is an underlying assumption of the hydrodynamic description. Larger $N_{\rm ch}$ implies a larger density $N_{\rm ch}/V$, as the volume V (Fig. 1) is essentially defined by the impact parameter, which is fixed. In hydrodynamics, one assumes that the system is locally thermalized, and larger density corresponds to higher initial temperature. Note that relativity plays an essential role in this correspondence. In nonrelativistic thermodynamics, density and temperature are independent variables. Heating a system at constant volume does not change its density because the number of particles is conserved. In a relativistic system, on the other hand, particles can be created by converting kinetic energy into mass, and a higher temperature implies a higher density. It also implies a higher energy per particle, which eventually results in a larger momentum per particle $[p_t]$ [4].

In order to illustrate that the positive correlation between $[p_t]$ and $N_{\rm ch}$ is not trivial, Fig. 3 also displays results of simulations using the HIJING model [29], in which particles do not interact after they are produced. The correlation is smaller by a factor ≈10. Note, however, that while thermalization always implies a positive correlation, the converse statement does not hold. In the color-glass condensate picture of high-energy collisions, such a correlation is already present at the level of particle production, since both the momentum per particle and the particle density increase with the saturation scale [33].

We now discuss the implications of thermalization on the observed $[p_t]$ fluctuations. First, note that the experimental analysis is done at fixed $N_{\rm ch}$, while our hydrodynamic simulation is done at fixed b. Both choices are dictated by practical reasons. Experimentally, b is not measured. In the simulation, on the other hand, one must define b before starting the simulation, while $N_{\rm ch}$ is only evaluated at the end.

In order to understand experimental results, we must reason at fixed $N_{\rm ch}$, where b varies. Larger b implies smaller collision volume V and larger density $N_{\rm ch}/V$, hence larger $[p_t]$ on average. We denote by $\overline{p_t}(N_{\rm ch}, b)$ the expectation value of $[p_t]$ at fixed $N_{\rm ch}$ and b. It increases with $N_{\rm ch}$ at fixed b, and with b at fixed $N_{\rm ch}$. In addition, there are fluctuations of $[p_t]$ even if both $N_{\rm ch}$ and b are fixed, as illustrated by the simulation in Fig. 3. We denote by $\mathrm{Var}(p_t|N_{\rm ch}, b)$ their variance. We then average over b at fixed $N_{\rm ch}$. The average value of $[p_t]$ is $\langle\overline{p_t}(N_{\rm ch}, b)\rangle_b$, where $\langle\cdots\rangle_b$ denotes an average over b. The average value of $[p_t]^2$ is $\langle\overline{p_t}(N_{\rm ch}, b)^2 + \mathrm{Var}(p_t|N_{\rm ch}, b)\rangle_b$. Therefore, the variance of $[p_t]$ is the sum of two positive terms:

$$\mathrm{Var}(p_t|N_{\rm ch}) = \left(\langle\overline{p_t}(N_{\rm ch}, b)^2\rangle_b - \langle\overline{p_t}(N_{\rm ch}, b)\rangle_b^2\right) + \langle\mathrm{Var}(p_t|N_{\rm ch}, b)\rangle_b, \quad (1)$$

The first term stems from the variation of $\overline{p_t}(N_{\rm ch}, b)$ with b. We refer to the second term as the intrinsic variance, in the sense that it is not a byproduct of b fluctuations. As we shall see, both terms are of comparable magnitudes, and the first term explains the peculiar pattern observed for large $N_{\rm ch}$.

We now carry out a quantitative calculation, which can be compared with data. First, precise information can be obtained, without any microscopic modeling, about the probability distribution of b at fixed $N_{\rm ch}$, $P(b|N_{\rm ch})$ [37]. This is achieved by solving first the inverse problem, namely, finding the probability distribution of $N_{\rm ch}$ for fixed b, $P(N_{\rm ch}|b)$, and then applying Bayes' theorem $P(b|N_{\rm ch})P(N_{\rm ch}) = P(N_{\rm ch}|b)P(b)$. As explained above, collisions at the same b differ by quantum fluctuations, which result in fluctuations of $N_{\rm ch}$. In nucleus-nucleus collisions, these fluctuations are Gaussian to a good approximation. They are characterized by the mean, $\overline{N_{\rm ch}}(b)$, and the variance, $\mathrm{Var}(N_{\rm ch}|b)$.

What one measures is the distribution $P(N_{\rm ch})$, obtained after integrating over all values of b, shown in Fig. 2(a), left. We only display values of $N_{\rm ch}$ larger than some threshold such that only 20% of the events are included, corresponding to fairly central collisions on which our analysis focuses. $P(N_{\rm ch})$ varies mildly up to $N_{\rm ch} \approx 3500$, then decreases steeply. By fitting it as a superposition of Gaussians, one can precisely reconstruct $\overline{N_{\rm ch}}(b)$ and $\mathrm{Var}(N_{\rm ch}|b = 0)$ [38] (see Supplemental Material [15], Sec. I). This fit is shown in Fig. 2(a). The knee of the distribution, defined as the mean value of $N_{\rm ch}$ for collisions at $b = 0$, is reconstructed precisely, and indicated as a vertical line. The steep fall of $P(N_{\rm ch})$ above the knee gives direct access to $\mathrm{Var}(N_{\rm ch}|b = 0)$. (Note that the variance is only reconstructed at $b = 0$, and one must resort to assumptions

[1] We only consider spherical nuclei. For deformed nuclei, one must also consider fluctuations in their orientations, which affect both the multiplicity [34] and the momentum per particle [35].

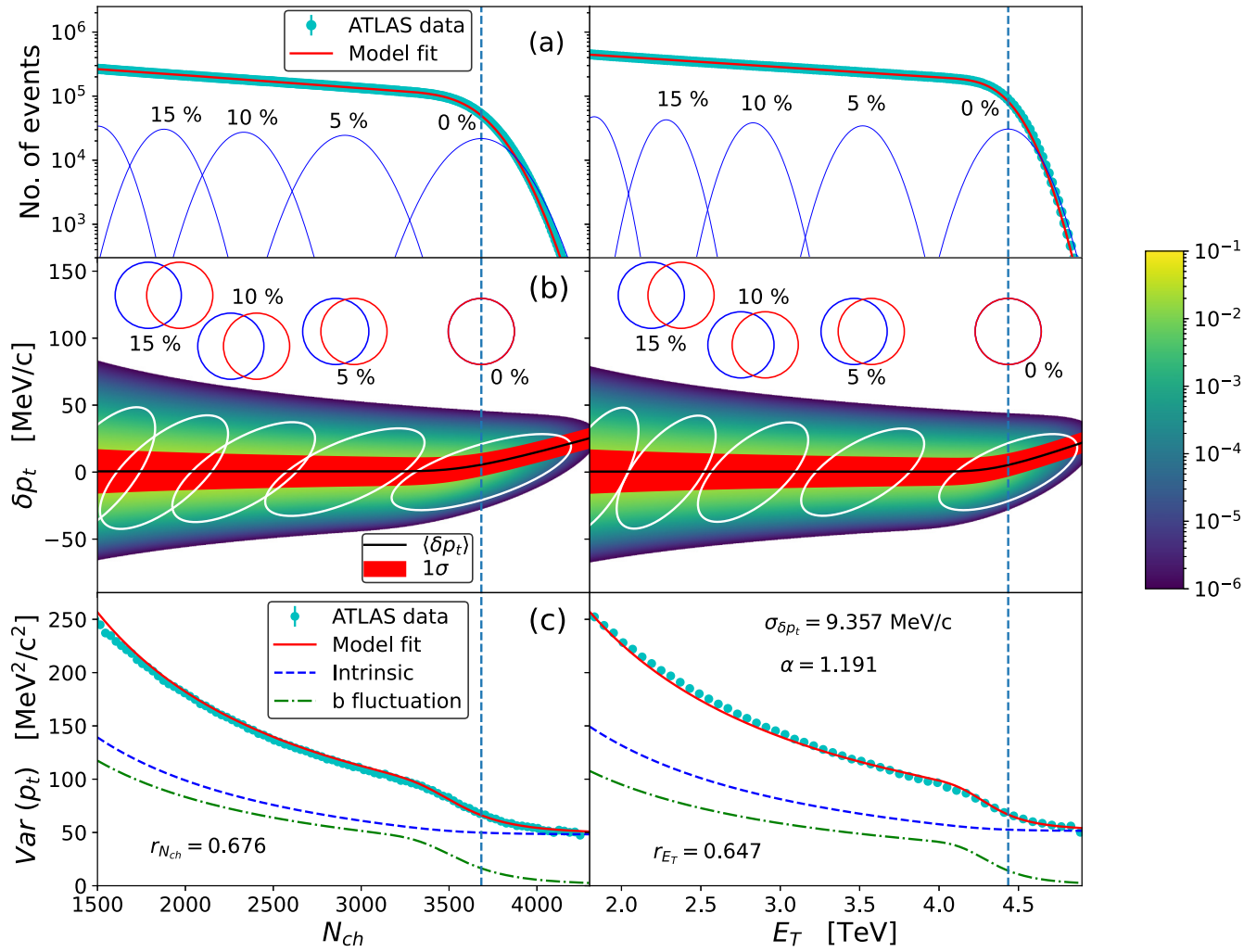

FIG. 2. (a) Histogram of the number of charged particles $N_{\rm ch}$ (left), measured in the inner detector of ATLAS, and of transverse energy E_T (right), measured in the forward and backward calorimeters. Solid lines are fits using superpositions of Gaussians. Contributions of collisions at fixed impact parameter b corresponding to centrality fractions 0, 5%, 10%, 15% are shown as thin blue lines (see Supplemental Material [15], Sec. I). The vertical dashed line corresponds to the knee, defined as the average value of $N_{\rm ch}$ or E_T for $b = 0$ collisions. (b) Joint distribution of the transverse momentum per particle $[p_t]$ and $N_{\rm ch}$ (or E_T) from our model. Rather than $[p_t]$, we plot the deviation $\delta p_t \equiv [p_t] - \overline{p_{t0}}$, where $\overline{p_{t0}}$ is the average value of p_t at fixed impact parameter, which is assumed to be constant. White curves are 99% confidence ellipses at fixed b. A schematic representation of the two colliding nuclei for these values of b is also shown (See Supplemental Material [15], Sec. I). The black line is the mean value of δp_t, and the red band is the 1-σ band. (c) Variance of the transverse momentum per particle $[p_t]$ as a function of the centrality estimator. The red solid line is the square of the half-width of the red band in (b). Symbols are ATLAS data [27]. We also display separately the two contributions to the variance, Eq. (1), in our model calculation, whose sum is the full line.

as to its dependence on b. We have checked that our results are robust with respect to these assumptions, see Supplemental Material [15], Secs. I and IV.) We refer to events above the knee as ultracentral collisions [39,40]. They are a small fraction of the total number of events, 0.35%, but ATLAS has recorded enough collisions that a few events are seen with values of $N_{\rm ch}$ larger than the knee by 20%, corresponding to four standard deviations. Note that Poisson fluctuations contribute only by 15% to the variance [38], so that the fluctuations of $N_{\rm ch}$ are mostly dynamical.

We then model the fluctuations of $[p_t]$. In the same way as we have assumed that the probability of $N_{\rm ch}$ at fixed b is Gaussian, we assume that the joint probability of $N_{\rm ch}$ and $[p_t]$, such as displayed in Fig. 3, is a two-dimensional Gaussian (see Supplemental Material [15], Sec. III). It is characterized by five quantities: The mean and variance of $[p_t]$ and $N_{\rm ch}$, which we denote by $\overline{p_t}(b)$, $\overline{N_{\rm ch}}(b)$, $\mathrm{Var}(p_t|b)$, $\mathrm{Var}(N_{\rm ch}|b)$, and the covariance or, equivalently, the Pearson correlation coefficient $r_{N_{\rm ch}}(b)$ between $[p_t]$ and $N_{\rm ch}$, which we expect to be positive as illustrated in Fig. 3. $\overline{N_{\rm ch}}(b)$ and $\mathrm{Var}(N_{\rm ch}|b)$ are obtained from the fit to $P(N_{\rm ch})$, as explained above. The mean transverse momentum is essentially independent of centrality for the 30% most central collisions [41], therefore, we assume that $\overline{p_t}(b)$ is independent of b, and we denote its value by $\overline{p_{t0}}$. Since we only evaluate the fluctuations around $\overline{p_{t0}}$, results are independent of its value. The variance $\mathrm{Var}(p_t|b)$ may have a nontrivial dependence on the impact parameter, but a smooth one. For statistical fluctuations, it is proportional to $1/N_{\rm ch}$. We

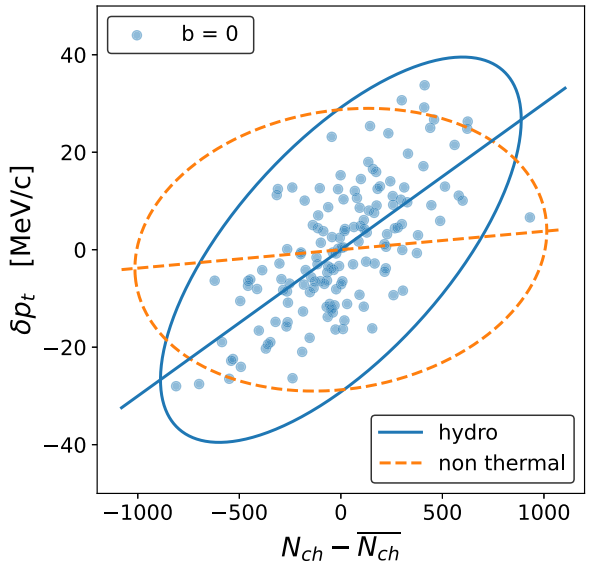

FIG. 3. Simulations of Pb+Pb collisions at 5.02 TeV and $b = 0$. The first set of simulations, shown as solid lines and symbols, consists of 150 collisions modeled using relativistic hydrodynamics [31]. The second set, shown as dashed lines, consists of 1.4×10^6 collisions simulated with HIJING [29], in which there is no thermalization mechanism. The figure represents the distribution of the charged particle multiplicity $N_{\rm ch}$ and the transverse momentum per particle $[p_t]$, where $N_{\rm ch}$ is calculated using the same acceptance cuts on θ and p_t as in the ATLAS analysis. We plot, rather than $N_{\rm ch}$ and $[p_t]$ themselves, the differences $N_{\rm ch} - \overline{N_{\rm ch}}$ and $\delta p_t \equiv [p_t] - \overline{p_t}$, where $\overline{N_{\rm ch}} = 6662$ and $\overline{p_t} = 1074$ MeV/c are the values averaged over collisions. The straight lines indicate the average value $\overline{\delta p_t}(N_{\rm ch}, b = 0)$, and the ellipses are 99% confidence ellipses [as in Fig. 2(b)]. Both are evaluated by assuming that the distribution is Gaussian (see Supplemental Material [15], Sec. III). Note that the fluctuations contain a contribution from statistical Poisson fluctuations in the HIJING model, which is a particle-based description, not in hydrodynamics, which is a continuous description (see Supplemental Material [15] Sec. II).

allow for a more general power-law dependence $\mathrm{Var}(p_t|b) = \sigma^2_{\delta p_t}(\overline{N_{\rm ch}}(0)/\overline{N_{\rm ch}}(b))^{\alpha}$, where $\sigma_{\delta p_t}$ and α are constants. Finally, we ignore the impact parameter dependence of the correlation coefficient $r_{N_{\rm ch}}$ for simplicity.

With this Gaussian ansatz, one can evaluate analytically the quantities entering the right-hand side of Eq. (1) as a function of the parameters of the Gaussian (see Supplemental Material [15], Sec. III), and the averages over b are evaluated using the probability distribution $P(b|N_{\rm ch})$ obtained using the Bayesian method outlined above (see Supplemental Material [15], Sec. I). The remaining three parameters ($\sigma_{\delta p_t}$, α, and $r_{N_{\rm ch}}$) are fitted to ATLAS data.

Let us first examine the distribution of $[p_t]$ and $N_{\rm ch}$ returned by our fit, which is represented in the left panel of Fig. 2(b). The white curves represent 99% confidence ellipses at fixed impact parameter [38]. One sees that they are tilted with respect to the horizontal axis, as in the hydrodynamic calculation of Fig. 3. This tilt reflects the positive correlation between $[p_t]$ and $N_{\rm ch}$, parameterized by $r_{N_{\rm ch}}$. As explained above, this correlation is a natural consequence of thermalization. The width of the $[p_t]$ distribution for fixed $N_{\rm ch}$ is due in part to the fact that several ellipses contribute for a given $N_{\rm ch}$ [first term in Eq. (1)], and in part to the vertical width of a single ellipse [second term in Eq. (1)].

The left panel of Fig. 2(c) displays the data and the model fit, as well as the two terms of Eq. (1). The model explains precisely the observed decrease of the variance around the knee. It comes from the first term, namely, from impact parameter fluctuations at fixed $N_{\rm ch}$, whose effect becomes negligible in ultracentral collisions. The magnitude of this term is essentially determined by the correlation coefficient $r_{N_{\rm ch}}$, which is thus constrained by data.

As a corollary, we predict a small increase in the average transverse momentum, represented as a black line in Fig. 2(b), in ultracentral collisions. This effect, which had been predicted a while ago [42,43], has recently been observed by CMS Collaboration [44]. Note that the increase is quantitatively predicted by our model calculation.

A specificity of the ATLAS analysis is that it uses, in addition to $N_{\rm ch}$, an alternative centrality estimator, which is the transverse energy E_T (defined as energy multiplied by $\sin\theta$) deposited in two calorimeters located symmetrically on both sides of the collision point, which cover roughly the ranges $1^\circ < \theta < 5^\circ$ and $175^\circ < \theta < 179^\circ$. The analysis of the variance is repeated by sorting events according to E_T, rather than $N_{\rm ch}$, and shown in the right panel of Fig. 2. In the same way, our model calculation can be repeated, replacing $N_{\rm ch}$ with E_T everywhere. This is a useful and nontrivial check of the validity of our approach. Even though the distributions of $N_{\rm ch}$ and E_T look similar in shape [Fig. 2(a)], the fall above the knee is steeper for E_T than for $N_{\rm ch}$, and there are only 0.26% of events above the knee for E_T, as opposed to 0.35% for $N_{\rm ch}$. It is interesting to notice that despite this significant difference, the decrease of the variance observed by ATLAS [Fig. 2(c)] still occurs around the knee. The parameters $\sigma_{\delta p_t}$ and α, which determine the dependence of the variance of $[p_t]$ on impact parameter, should not depend on whether one classifies events according to $N_{\rm ch}$ or E_T. We determine the values that give the best simultaneous agreement with $N_{\rm ch}$ and E_T-based data (see Supplemental Material [15] Sec. IV). The Pearson correlation coefficient r_{E_T} between $[p_t]$ and E_T need not coincide with $r_{N_{\rm ch}}$ and is fitted independently. Note that $r_{N_{\rm ch}}$ corresponds to the correlation between $[p_t]$ and $N_{\rm ch}$ for the same particles, while r_{E_T} represents the correlation between $[p_t]$ and the E_T measured in different angular windows. One therefore expects $r_{E_T} < r_{N_{\rm ch}}$, which is confirmed by our fit. Values, however, are very similar, which shows that particle depositions in different θ windows are very strongly correlated.

We have revealed a new effect of thermalization, which involves the momenta of particles, rather than their direction. It is spectacular because of its unique centrality dependence (as opposed to the presence of excess photons, also interpreted as resulting from thermal production [45,46]). Our study thus highlights the importance of impact parameter, which defines the geometry and is an essential ingredient of the hydrodynamic description: The momentum per particle depends on its magnitude, much in the same way as elliptic flow is driven by its orientation. It is interesting to note that the impact parameter is a classical quantity, in the sense that

its quantum uncertainty is negligible: Heisenberg's principle gives $\delta b \equiv \hbar/P \approx 4 \times 10^{-7}$ fm for a Pb+Pb collision at the LHC, negligible compared to the range spanned by b, of order 15 fm.[2] It is actually the only classical quantity characterizing a collision, and collisions with the same impact parameter differ only by quantum fluctuations. Due to the high energy of the collision, however, a single quantum fluctuation can produce a large number of particles, which promotes it to the status of a classical fluctuation. (Elliptic flow in central collisions [47] and triangular flow [48] are driven by a similar mechanism.) The effect studied in this Letter involves a subtle interplay between classical fluctuations of impact parameter, and quantum fluctuations of the collision multiplicity.

[2]Note that in event-by-event simulations, the impact parameter is correctly defined only if each nucleus is recentered after randomly drawing nucleon positions. The recentering correction is larger by orders of magnitude than the quantum uncertainty. It is not implemented in the simulations shown in Fig. 3, but this does not alter the conclusions drawn from this figure.

We thank the Institute for Nuclear Theory at the University of Washington for hosting the program "Intersection of nuclear structure and high-energy nuclear collisions" during which this work was initiated. We thank Govert Nijs and Wilke van der Schee for the discussions, and Jean-Paul Blaizot for useful comments on the manuscript. R.S. is supported by the Polish National Science Center under grant NAWA PRELUDIUM BIS: PPN/STA/2021/1/00040/U/00001 and PRELUDIUM BIS: 2019/35/O/ST2/00357. S.B. and J.J. are supported by DOE DE-FG02-87ER40331 and DE-SC0024602. M.L. thanks the São Paulo Research Foundation (FAPESP) for support under Grants No. 2021/08465-9, No. 2018/24720-6, and No. 2017/05685-2, as well as the support of the Brazilian National Council for Scientific and Technological Development (CNPq). We acknowledge support from the "Emilie du Châtelet" visitor programme and from the GLUODYNAMICS project funded by the "P2IO LabEx (ANR-10-LABX-0038)" in the framework "Investissements d'Avenir" (ANR-11-IDEX-0003-01) managed by the Agence Nationale de la Recherche (ANR).

[1] W. Busza, K. Rajagopal, and W. van der Schee, Heavy ion collisions: The big picture, and the big questions, Annu. Rev. Nucl. Part. Sci. **68**, 339 (2018).
[2] B. Schenke, The smallest fluid on Earth, Rep. Prog. Phys. **84**, 082301 (2021).
[3] J. Adam *et al.* (ALICE Collaboration), Centrality dependence of the pseudorapidity density distribution for charged particles in Pb-Pb collisions at $\sqrt{s_{\rm NN}} = 5.02$ TeV, Phys. Lett. B **772**, 567 (2017).
[4] F. G. Gardim, G. Giacalone, M. Luzum, and J.-Y. Ollitrault, Thermodynamics of hot strong-interaction matter from ultrarelativistic nuclear collisions, Nat. Phys. **16**, 615 (2020).
[5] E. Shuryak, Why does the quark gluon plasma at RHIC behave as a nearly ideal fluid? Prog. Part. Nucl. Phys. **53**, 273 (2004).
[6] K. H. Ackermann *et al.* (STAR Collaboration), Elliptic flow in Au + Au collisions at $\sqrt{s_{NN}} = 130$ GeV, Phys. Rev. Lett. **86**, 402 (2001).
[7] K. Aamodt *et al.* (ALICE Collaboration), Elliptic flow of charged particles in Pb-Pb collisions at 2.76 TeV, Phys. Rev. Lett. **105**, 252302 (2010).
[8] C. Gale, S. Jeon and B. Schenke, Hydrodynamic modeling of heavy-ion collisions, Int. J. Mod. Phys. A **28**, 1340011 (2013).
[9] B. B. Back *et al.* (PHOBOS Collaboration), Charged-particle multiplicity near midrapidity in central $Au + Au$ collisions at $\sqrt{s_{NN}} = 56$ and 130 GeV, Phys. Rev. Lett. **85**, 3100 (2000).
[10] C. Adler *et al.* (STAR Collaboration), Multiplicity distribution and spectra of negatively charged hadrons in Au + Au collisions at $\sqrt{s_{NN}} = 130$ GeV, Phys. Rev. Lett. **87**, 112303 (2001).
[11] S. S. Adler *et al.* (PHENIX Collaboration), Systematic studies of the centrality and $\sqrt{s_{NN}}$ dependence of the $dE_T/d\eta$ and $dN_{\rm ch}/d\eta$ in heavy ion collisions at midrapidity, Phys. Rev. C **71**, 034908 (2005); S. S. Adler *et al.*, Publisher's note: Systematic studies of the centrality and $\sqrt{s_{NN}}$ dependence of the $dE_T/d\eta$ and $dN_{\rm ch}/d\eta$ in heavy ion collisions at mid-rapidity [Phys. Rev. C 71, 034908 (2005)], **71**, 049901 (2005).
[12] B. Abelev *et al.* (ALICE Collaboration), Centrality determination of Pb-Pb collisions at $\sqrt{s_{NN}} = 2.76$ TeV with ALICE, Phys. Rev. C **88**, 044909 (2013).
[13] J. Adams *et al.* (STAR Collaboration), Event by event $\langle p_t \rangle$ fluctuations in Au-Au collisions at $\sqrt{s_{NN}} = 130$ GeV, Phys. Rev. C **71**, 064906 (2005).
[14] B. B. Abelev *et al.* (ALICE Collaboration), Event-by-event mean $p_{\rm T}$ fluctuations in pp and Pb-Pb collisions at the LHC, Eur. Phys. J. C **74**, 3077 (2014).
[15] See Supplemental Material at http://link.aps.org/supplemental/10.1103/PhysRevC.109.L051902 for details about the Bayesian reconstruction of impact parameter, the Monte Carlo simulations with hydrodynamics and HIJING, the two-dimensional Gaussian parametrization of fluctuations, and the fits to ATLAS data, which includes Refs. [16–26].
[16] J. F. Paquet, C. Shen, G. S. Denicol, M. Luzum, B. Schenke, S. Jeon, and C. Gale, Production of photons in relativistic heavy-ion collisions, Phys. Rev. C **93**, 044906 (2016).
[17] J. S. Moreland, J. E. Bernhard, and S. A. Bass, Alternative ansatz to wounded nucleon and binary collision scaling in high-energy nuclear collisions, Phys. Rev. C **92**, 011901(R) (2015).
[18] J. Adam *et al.* (ALICE Collaboration), Centrality dependence of the charged-particle multiplicity density at midrapidity in Pb-Pb collisions at $\sqrt{s_{\rm NN}} = 5.02$ TeV, Phys. Rev. Lett. **116**, 222302 (2016).
[19] E. Grossi, A. Soloviev, D. Teaney, and F. Yan, Soft pions and transport near the chiral critical point, Phys. Rev. D **104**, 034025 (2021).
[20] A. Guillen and J.-Y. Ollitrault, Fluid velocity from transverse momentum spectra, Phys. Rev. C **103**, 064911 (2021).
[21] P. Bożek and W. Broniowski, Transverse-momentum fluctuations in relativistic heavy-ion collisions from event-by-event viscous hydrodynamics, Phys. Rev. C **85**, 044910 (2012).

[22] P. Bożek and W. Broniowski, Transverse momentum fluctuations in ultrarelativistic Pb + Pb and p + Pb collisions with 'wounded' quarks, Phys. Rev. C **96**, 014904 (2017).

[23] J. E. Bernhard, J. S. Moreland, and S. A. Bass, Bayesian estimation of the specific shear and bulk viscosity of quark–gluon plasma, Nat. Phys. **15**, 1113 (2019).

[24] D. Everett *et al.* (JETSCAPE Collaboration), Multisystem Bayesian constraints on the transport coefficients of QCD matter, Phys. Rev. C **103**, 054904 (2021).

[25] F. G. Gardim, F. Grassi, P. Ishida, M. Luzum, and J.-Y. Ollitrault, p_T-dependent particle number fluctuations from principal-component analyses in hydrodynamic simulations of heavy-ion collisions, Phys. Rev. C **100**, 054905 (2019).

[26] S. Acharya *et al.* (ALICE Collaboration), Transverse momentum spectra, and nuclear modification factors of charged particles in pp, p-Pb and Pb-Pb collisions at the LHC, J. High Energy Phys. 11 (2018) 013.

[27] G. Aad *et al.* (ATLAS Collaboration), Correlations between flow and transverse momentum in Xe+Xe and Pb+Pb collisions at the LHC with the ATLAS detector: A probe of the heavy-ion initial state and nuclear deformation, Phys. Rev. C **107**, 054910 (2023).

[28] X.-N. Wang and M. Gyulassy, HIJING: A Monte Carlo model for multiple jet production in pp, pA and AA collisions, Phys. Rev. D **44**, 3501 (1991).

[29] M. Gyulassy and X.-N. Wang, HIJING 1.0: A Monte Carlo program for parton and particle production in high-energy hadronic and nuclear collisions, Comput. Phys. Commun. **83**, 307 (1994).

[30] S. Bhatta, C. Zhang, and J. Jia, Higher-order transverse momentum fluctuations in heavy-ion collisions, Phys. Rev. C **105**, 024904 (2022).

[31] P. Bożek and R. Samanta, Factorization breaking for higher moments of harmonic flow, Phys. Rev. C **105**, 034904 (2022).

[32] M. L. Miller, K. Reygers, S. J. Sanders, and P. Steinberg, Glauber modeling in high energy nuclear collisions, Annu. Rev. Nucl. Part. Sci. **57**, 205 (2007).

[33] F. Gelis, E. Iancu, J. Jalilian-Marian, and R. Venugopalan, The color glass condensate, Annu. Rev. Nucl. Part. Sci. **60**, 463 (2010).

[34] L. Adamczyk *et al.* (STAR Collaboration), Azimuthal anisotropy in U + U and Au + Au collisions at RHIC, Phys. Rev. Lett. **115**, 222301 (2015).

[35] G. Giacalone, Observing the deformation of nuclei with relativistic nuclear collisions, Phys. Rev. Lett. **124**, 202301 (2020).

[36] C. E. Aguiar, Y. Hama, T. Kodama, and T. Osada, Event-by-event fluctuations in hydrodynamical description of heavy ion collisions, Nucl. Phys. A **698**, 639 (2002).

[37] S. J. Das, G. Giacalone, P. A. Monard, and J.-Y. Ollitrault, Relating centrality to impact parameter in nucleus-nucleus collisions, Phys. Rev. C **97**, 014905 (2018).

[38] K. V. Yousefnia, A. Kotibhaskar, R. Bhalerao, and J.-Y. Ollitrault, Bayesian approach to long-range correlations and multiplicity fluctuations in nucleus-nucleus collisions, Phys. Rev. C **105**, 014907 (2022).

[39] M. Luzum and J.-Y. Ollitrault, Extracting the shear viscosity of the quark-gluon plasma from flow in ultra-central heavy-ion collisions, Nucl. Phys. A **904-905**, 377c (2013).

[40] S. Chatrchyan *et al.* (CMS Collaboration), Studies of Azimuthal dihadron correlations in ultra-central PbPb collisions at $\sqrt{s_{NN}} = 2.76$ TeV, J. High Energ. Phys. 02 (2014) 088.

[41] S. Acharya *et al.* (ALICE Collaboration), Transverse momentum spectra and nuclear modification factors of charged particles in Xe-Xe collisions at $\sqrt{s_{\rm NN}} = 5.44$ TeV, Phys. Lett. B **788**, 166 (2019).

[42] F. G. Gardim, G. Giacalone, and J.-Y. Ollitrault, The mean transverse momentum of ultracentral heavy-ion collisions: A new probe of hydrodynamics, Phys. Lett. B **809**, 135749 (2020).

[43] G. Nijs and W. van der Schee, Predictions and postdictions for relativistic lead and oxygen collisions with the computational simulation code Trajectum, Phys. Rev. C **106**, 044903 (2022).

[44] C. A. Bernardes, Extracting the speed of sound in the strongly interacting matter created in relativistic nuclear collisions with the CMS experiment, arXiv:2312.11758.

[45] B. Alver *et al.* (PHOBOS Collaboration), System size, energy, pseudorapidity, and centrality dependence of elliptic flow, Phys. Rev. Lett. **98**, 242302 (2007).

[46] B. Alver and G. Roland, Collision geometry fluctuations and triangular flow in heavy-ion collisions, Phys. Rev. C **81**, 054905 (2010); **82**, 039903(E) (2010).

[47] M. Wilde (ALICE Collaboration), Measurement of direct photons in pp and Pb-Pb collisions with ALICE, Nucl. Phys. A **904-905**, 573c (2013).

[48] A. Adare *et al.* (PHENIX Collaboration), Centrality dependence of low-momentum direct-photon production in Au + Au collisions at $\sqrt{s_{NN}} = 200$ GeV, Phys. Rev. C **91**, 064904 (2015).